PCCP

ROYAL SOCIETY OF CHEMISTRY

PAPER

View Article Online
View Journal

Cite this: DOI: 10.1039/d0cp02665d

How does methylviologen cation radical supply two electrons to the formate dehydrogenase in the catalytic reduction process of CO_2 to formate?

Akimitsu Miyaji*[a] and Yutaka Amao *[bc]

Received 16th May 2020,
Accepted 22nd July 2020

DOI: 10.1039/d0cp02665d

rsc.li/pccp

Formate dehydrogenase from *Candida boidinii* (EC.1.2.1.2; CbFDH) is a commercially available enzyme and can be easily handled as a catalyst for the CO_2 reduction to formate in the presence of NADH, single-electron reduced methylviologen ($MV^{+\bullet}$) and so on. It was found that the formate oxidation to CO_2 with CbFDH was suppressed using the oxidized MV as a co-enzyme and the single-electron reduced MV ($MV^{+\bullet}$) was effective for the catalytic activity of CbFDH for the CO_2 reduction to formate compared with that using the natural co-enzyme of NADH [Y. Amao, *Chem. Lett.*, 2017, **46**, 780–788]. The CO_2 reduction to formate catalyzed by CbFDH requires two molecules of the $MV^{+\bullet}$. In order to clarify the two-electron reduction process using $MV^{+\bullet}$ in the CO_2 reduction to formate catalyzed with CbFDH, we attempted enzyme reaction kinetics, electrochemical and quantum chemical analyses. Kinetic parameters obtained from the enzymatic kinetic analysis metric revealed an index of affinity of $MV^{+\bullet}$ for CbFDH in the CO_2 reduction to formate. From the results of the electrochemical analysis, it was predicted that only one molecule of $MV^{+\bullet}$ was bound to CbFDH, and the MV bound to CbFDH was to be necessarily re-reduced by the electron source outside of CbFDH to supply the second electron in the CO_2 reduction to formate. From the results of docking simulation and density functional theory (DFT) calculations, it was indicated that one molecule of MV bound to the position close to CO_2 in the inner part of the substrate binding pocket of CbFDH contributed to the two-electron CO_2 reduction to formate.

Introduction

Formate dehydrogenases (FDHs) are a set of enzymes that catalyze formate oxidation to CO_2, donating the electrons to a second substrate, and the CO_2 reduction to formate requires electron donation from a second substrate.[1–6] Among these FDHs, FDH from *Candida boidinii* (EC.1.2.1.2; CbFDH) is commercially available and can be easily handled as a catalyst for the CO_2 reduction to formate. CbFDH catalyzes formate oxidation to CO_2 and CO_2 reduction to formate with the redox coupling of NAD^+/NADH as shown in the following equation.

$$CO_2 + NADH + H^+ \overset{\text{CbFDH}}{\rightleftarrows} HCO_2H + NAD^+$$

Thus, CbFDH is an attractive biocatalyst for CO_2 reduction to formate. For example, as solar fuel production based on CO_2 reduction has received considerable attention, CbFDH is used as a catalyst for the visible-light-driven redox system consisting of an electron donor (D), a photosensitizer (P), an electron carrier (C) and CbFDH as shown in Fig. 1. In general, NAD^+ is not directly reduced to NADH with a metal complex-based photosensitizer. By incorporating a rhodium complex as a catalyst for hydride production into this system, it is possible to architect a visible-light-driven NAD^+ to NADH reduction system and accomplish CO_2 reduction to formate using CbFDH.[7–14]

Here, let us focus on the catalytic activity of CbFDH for formate oxidation or CO_2 reduction with NAD^+/NADH redox coupling. For example, the kinetic parameters for the Michaelis constant (K_m) values of NAD^+ and NADH for CbFDH in the formate oxidation to CO_2 and the reverse reaction are determined. The K_m values for NAD^+ in the formate oxidation and NADH in the CO_2 reduction to CbFDH are estimated to be 50 and 2087 mM, respectively.[6,15,16] Thus, CbFDH can be activated by the lower concentration of NAD^+, compared with that of NADH, and the affinity of NAD^+ for CbFDH is higher than that of NADH. Even if the effective NAD^+ reduction to NADH with the photoredox system could be achieved, NAD^+ is a very expensive biological material and, it is necessary to improve

---

[a] School of Materials and Chemical Technology, Tokyo Institute of Technology, 4259 G1-14, Nagatsuda, Midori-Ku, Yokohama 226-8502, Japan
[b] Graduate School of Science, Osaka City University, 3-3-138 Sugimoto, Sumiyoshi-ku, Osaka 558-8585, Japan. E-mail: amao@ocarina.osaka-cu.ac.jp
[c] Research Centre of Artificial Photosynthesis (ReCAP), Osaka City University, 3-3-138 Sugimoto, Sumiyoshi-ku, Osaka 558-8585, Japan

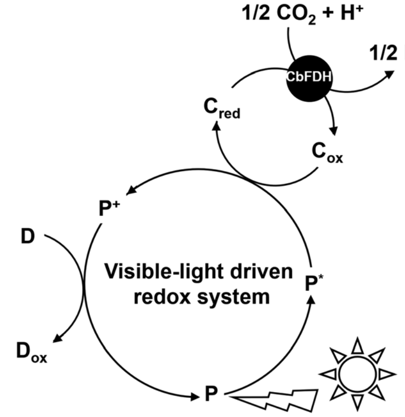

Fig. 1 Visible-light-driven CO_2 reduction to formate with the redox system consisting of an electron donor (D), a photosensitizer (P), an electron carrier (C) and CbFDH. C_{ox} and C_{red} indicate the oxidized and single-electron reduced electron carriers, respectively.

its usage and turnover of the redox coupling of NAD^+/NADH. As long as the redox coupling of NAD^+/NADH is used, the affinity between NAD^+ or NADH and CbFDH does not change, thus, CbFDH catalytic activity cannot be controlled in the photoredox system. As the produced NADH acts as a sacrificial reagent and is consumed, moreover, the redox coupling of NAD^+/NADH is not suitable for use in the photoredox system.

In contrast, the visible-light-driven CO_2 reduction to formate systems with the coupling of the photoreduction of various 4,4′- or 2,2′-bipyridinium salts (4,4′- or 2,2′-BPs) with ruthenium polypyridyl complex, water soluble zinc porphyrin or chlorophyll-*a* and CbFDH has been reported.[17–32] Furthermore, the effects of the chemical structures and redox potentials of various 2,2′-BPs on the CO_2 reduction to formate were reported.26 In this reaction, the single-electron reduced 4,4′- or 2,2′-BPs act as a co-enzyme for CbFDH instead of NADH. Representative example of 4,4′-BP single-electron reduction of methyl viologen (MV) with sodium dithionite produces a radical species as shown in Fig. 2.

Recently, we reported the kinetic parameters of various single-electron reduced 4,4′-BPs for CO_2 reduction to formate with CbFDH by using enzymatic kinetic analysis for the first time. We also elucidated that the formate oxidation to CO_2 with CbFDH is suppressed using oxidized 4,4′- or 2,2′-BP and the single-electron reduced 4,4′- or 2,2′-BP was effective in the catalytic activity of CbFDH for CO_2 reduction to formate, as shown in the following equation.[33–38]

$$CO_2 + 2BP^{+\bullet} + 2H^+ \xrightarrow{\text{CbFDH}} HCO_2H + 2BP$$

On the other hand, as shown in the reaction equation, the CO_2 reduction to formate catalyzed by CbFDH requires two molecules of the single-electron reduced BP ($BP^{+\bullet}$). In addition to the kinetic parameters, elucidation of the $BP^{+\bullet}$ to CbFDH will contribute to the design and the architecture of the highly active co-enzyme for CbFDH.

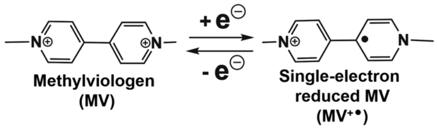

Fig. 2 Redox scheme for methylviologen (MV).

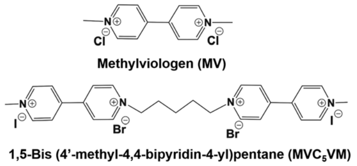

Fig. 3 Chemical structures of methylviologen (MV) and 1,5-bis (4′-methyl-4,4-bipyridin-4-yl)pentane (MVC_5VM).

In this article, to clarify the two-electron supply mechanism from single-electron reduced BP to CbFDH, we studied the extended enzymatic kinetic analysis for the CO_2 reduction to formate catalyzed by CbFDH using the dithionite-induced single-electron reduced methylviologen ($MV^{+\bullet}$) and a dimeric 4,4′-BP, 1,5-bis(4′-methyl-4,4-bipyridin-4-yl)pentane (MVC_5VM; chemical structure is shown in Fig. 3). We also investigated the mechanism of CO_2 reduction to formate using electrochemically reduced MV and CbFDH that are free of the reducing agent sodium dithionite. Furthermore, the interaction between $MV^{+\bullet}$ and CbFDH was clarified by docking simulation, and electron transfer ability was evaluated based on density functional theory (DFT) calculations.

Results and discussion

Analysis of enzymatic kinetics based on the Michaels–Menten and Hill equations

First, Michaels–Menten-type enzymatic kinetics for the CbFDH-catalyzed CO_2 reduction to formate using dithionite-reduced MV and MVC_5VM was analyzed. For analysis of enzyme kinetics, the CO_2 reduction to formate with $MV^{+\bullet}$ or $MV^{+\bullet}C_5^{\bullet+}VM$ and CbFDH was conducted under the following conditions. Sample solution consisted of MV or MVC_5VM, sodium dithionite (160 mM) and FDH (7.5 μM) in CO_2-saturated 50 mM sodium pyrophosphate buffer (pH 7.0). The concentration of formate was measured for 1 min to estimate the initial rate (v_0) of the CO_2 reduction to formate. The amount of formate production in this system was measured by ionic chromatography. Fig. 3 shows the relationship between the initial rate of formate production and concentration of $MV^{+\bullet}$ and $MV^{+\bullet}C_5^{\bullet+}VM$.

$$\nu = \frac{V_{\max}[\text{Viologen radical}]}{K_m + [\text{Viologen radical}]}$$

The initial rate of formate production increased with increasing concentrations of $MV^{+\bullet}$ or $MV^{+\bullet}C_5^{+\bullet}VM$ and then reached constant values; each plot obeyed the following Michaelis–Menten equation.

Here, $V_{\max}$ and apparent K_m are maximum velocity and Michaelis constant, respectively. The $V_{\max}$ and apparent K_m values were determined by the curve fitting using the Michaelis–Menten equation. From the results of the curve fitting, the apparent

K_m and V_{max} for the $MV^{+\bullet}$ were estimated to be 223 μM and 18.2 μM min^{-1}, respectively. In contrast, the apparent K_m and V_{max} for $MV^{+\bullet}C_5{}^{+\bullet}VM$ were estimated to be 191 μM and 17.7 μM min^{-1}, respectively. The turnover number termed k_{cat} is estimated by dividing V_{max} by the CbFDH concentration. Thus, k_{cat} values for $MV^{+\bullet}$ and $MV^{+\bullet}C_5{}^{+\bullet}VM$ were estimated to be 2.43 and 2.36 min^{-1}, respectively. The values of catalytic efficiency termed k_{cat}/K_m for $MV^{+\bullet}$ and $MV^{+\bullet}C_5{}^{+\bullet}VM$ were estimated to be 0.011 and 0.012 μM^{-1} min^{-1}, respectively. Here, two molecules of $MV^{+\bullet}$ are required in the CO_2 reduction to formate catalyzed by CbFDH. When two molecules of $MV^{+\bullet}$ are simultaneously bound to CbFDH, the Michaelis–Menten equation can be approximately regarded as the following equation.

$$\nu = \frac{0.5V_{max}[\text{Viologen radical}]}{K_m + [\text{Viologen radical}]}$$

From the results of the curve fitting using this equation, the apparent K_m and V_{max} for the single-electron reduced MV were estimated to be 223 μM and 36.4 μM min^{-1}, respectively. From this result, the k_{cat} and k_{cat}/K_m values for $MV^{+\bullet}$ were estimated to be 4.85 min^{-1} and 0.022 μM^{-1} min^{-1}, respectively. The reaction mechanism for CO_2 reduction to formate catalyzed by CbFDH with $MV^{+\bullet}$ is shown in Fig. 5.

It is known that $MV^{+\bullet}$ forms a complex with two molecules,[39–48] and considering the mechanism of Fig. 5, it is expected to bind to the active site of CbFDH as an $MV^{+\bullet}$ complex. Here, the dithionite reduction scheme in MVC_5VM with two viologen moieties is shown in Fig. 6. It is also known that $MV^{+\bullet}C_5{}^{+\bullet}VM$ forms a complex between viologen cation radical sites in the molecule,[49] and it is expected that the viologen cation radical complex site binds to the active site of CbFDH as shown in Fig. 7.

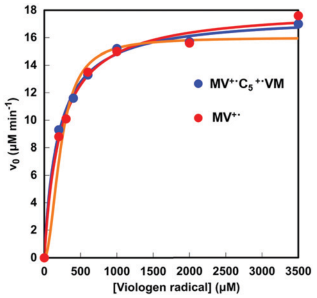

Fig. 4 The relationship between the concentration of $MV^{+\bullet}$ (blue) or $MV^{+\bullet}C_5{}^{+\bullet}VM$ (red) and the initial rate of formate production (v_0). Blue and red lines indicate the curve fitting using the Michaels–Menten equation. Orange line indicates the curve fitting using the Hill equation. Reaction conditions: MV or MVC_5VM, sodium dithionite (160 mM) and FDH (7.5 μM) in CO_2-saturated 50 mM sodium pyrophosphate buffer (pH 7.0).

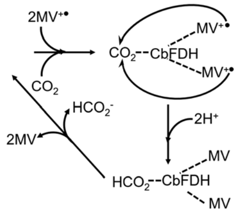

Fig. 5 Reaction mechanism for CO_2 reduction to formate catalyzed by CbFDH with two molecules of $MV^{+\bullet}$.

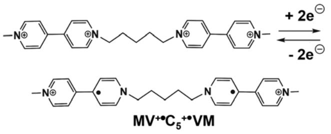

Fig. 6 Redox scheme for MVC_5VM with two viologen moieties.

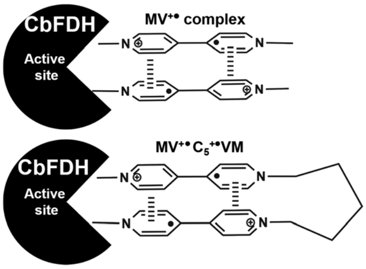

Fig. 7 Possible mechanism for viologen cation radical complex bound to the active site of CbFDH.

By using sodium dithionite as a reducing agent, each of the two viologen sites in MVC_5VM is reduced by single electrons, resulting in two radicals in the molecule ($MV^{+\bullet}C_5{}^{+\bullet}VM$). Thus, the reaction mechanism for CO_2 reduction to formate catalyzed by CbFDH with $MV^{+\bullet}C_5{}^{+\bullet}VM$ is shown in Fig. 8.

It is expected that the apparent K_m value of $MV^{+\bullet}C_5{}^{+\bullet}VM$ for CbFDH will be half of that of $MV^{+\bullet}$ in the CO_2 reduction as shown in Fig. 8. However, there is no significant difference in K_m value for CbFDH between $MV^{+\bullet}C_5{}^{+\bullet}VM$ and MV in the CO_2 reduction. Therefore, even when $MV^{+\bullet}C_5{}^{+\bullet}VM$ is used, the CO_2 reduction to formate using CbFDH does not proceed with only one molecule of $MV^{+\bullet}C_5{}^{+\bullet}VM$, and as with $MV^{+\bullet}$, two molecules of $MV^{+\bullet}C_5{}^{+\bullet}VM$ are required. Kinetic parameters obtained from the enzymatic kinetic analysis metric revealed an index of affinity of $MV^{+\bullet}$ or $MV^{+\bullet}C_5{}^{+\bullet}VM$ for CbFDH in the CO_2 reduction to formate.

When two molecules of $MV^{+\bullet}$ are sequentially bound to CbFDH, the reaction mechanism for CO_2 reduction to formate catalyzed by CbFDH with $MV^{+\bullet}$ is shown in Fig. 9.

In this reaction mechanism, the CO_2 reduction to formate obeyed the following Hill equation.

$$\nu = \frac{V_{max}([\text{Viologen radical}]/K_m)^2}{1 + ([\text{Viologen radical}]/K_m)^2}$$

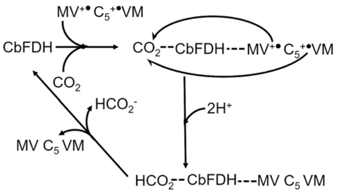

Fig. 8 Reaction mechanism for CO_2 reduction to formate catalyzed by CbFDH with $MV^{+\bullet}C_5{}^{+\bullet}VM$.

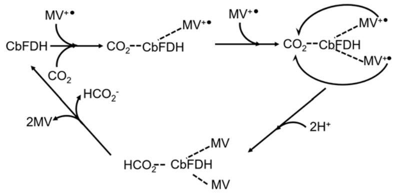

Fig. 9 Reaction mechanism for CO_2 reduction to formate catalyzed by CbFDH with two sequentially bound molecules of $MV^{+\bullet}$.

The orange line in Fig. 4 indicates the curve fitting using Hill equation for $MV^{+\bullet}$. From the results of the curve fitting using this equation, the apparent K_m and V_{max} for $MV^{+\bullet}$ in the CO_2 reduction to formate with CbFDH were estimated to be 226 μM and 15.8 μM min^{-1}, respectively.

However, in this reaction system, sodium dithionite is excessive as a reducing agent. The following control experiments were conducted to investigate the possibility of direct reduction of CO_2 to formate with sodium dithionite. First, sodium dithionite (concentration: 0, 50, 100 and 150 mM) was added to the CO_2-saturated 50 mM sodium pyrophosphate buffer (pH 7.0) and then incubated at 30.5 °C for 1 h. No formate production was observed under the condition of sodium dithionite concentration (0–150 mM). Moreover, MV (concentration: 0–3.5 mM) and sodium dithionite (160 mM), in the absence of CbFDH, were added to the CO_2-saturated 50 mM sodium pyrophosphate buffer (pH 7.0) and then incubated at 30.5 °C for 1 h. Also, no formate production was observed under these conditions. In all the cases, it was confirmed that the concentrations of CO_2 and bicarbonate ion in the solution measured by ionic chromatography were unchanged during the incubation. These results suggest that direct reduction of CO_2 to formate with sodium dithionite did not proceed.

In order to investigate the possibility of direct electron transfer from sodium dithionite to CbFDH, CO_2 reduction to formate in sodium pyrophosphate buffer (pH 7.0) without MV was attempted. The sample solution consisted of sodium dithionite and FDH (7.5 μM) in CO_2-saturated 50 mM sodium pyrophosphate buffer (pH 7.0). In this test, the sodium dithionite concentration was varied from 0 to 150 mM. After 1 h incubation at 30.5 °C, no formate production was observed and the concentrations of CO_2 and bicarbonate ion in the solution were unchanged during the incubation.

It is still possible that MV bound to CbFDH is again reduced by sodium dithionite and finally supplies two electrons to CbFDH. Therefore, the analysis of the reaction using dithionite-reduced MV does not lead to the elucidation of the two-electron supply mechanism from $MV^{+\bullet}$ to CbFDH.

CO_2 reduction to formate catalyzed with CbFDH using electrochemically single-electron-reduced MV

In order to eliminate the influence of excess sodium dithionite in the reaction system, the CO_2 reduction to formate catalyzed by CbFDH was investigated using electrochemically single-electron-reduced MV. First, the electrochemical analysis for CO_2 reduction to formate catalyzed by CbFDH using $MV^{+\bullet}$ is investigated.

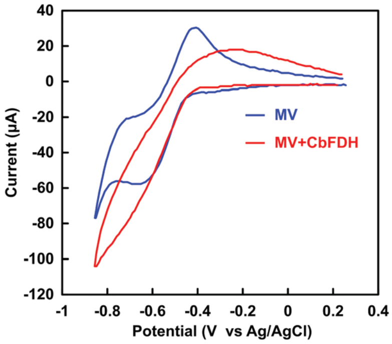

Fig. 10 Cyclic voltammograms for MV (blue) and MV + CbFDH (red) in CO_2-saturated 0.1 M phosphate buffer (pH 6.8).

Fig. 10 shows the cyclic voltammograms (CV) for MV (blue) and MV coexisting with CbFDH (MV + CbFDH; red) in CO_2 saturated 0.1 M phosphate buffer (pH 6.8). For CV measurement, grassy carbon, platinum wire and Ag/AgCl electrodes were used as working, counter and reference electrodes, respectively. The first reduction potential for MV was estimated to be −660 mV. On the other hand, a sigmoidal and steady-state cathodic wave was observed in CO_2 saturated 0.1 M phosphate buffer containing MV and CbFDH. From the results of Fig. 10, in contrast, the peak current of MV coexisting with CbFDH was larger than that of MV in the CV measurement. Similar catalytic current observation has been reported for CV measurement of a solution containing MV, bicarbonate, and W-containing FDH.[50] Thus, the increase in current corresponds to the catalytic current based on CO_2 reduction in the presence of CbFDH.

Next, the CO_2 reduction to formate was investigated by applying a constant potential (−660 mV *vs.* Ag/AgCl) to a CO_2 saturated-buffer containing MV and CbFDH. In constant potential CO_2 reduction to formate using CbFDH and MV, an H-type electrochemical cell as shown in Fig. 11 was used.

Platinum wire, carbon fabric paper (CFP) (TGP-H-030 obtained from TORAY INDUSTRIES, INC.; electrode area: 3.75 cm^2) and Ag/AgCl electrodes were used as an anode, a cathode and a reference electrode, respectively. The CO_2 saturated phosphate buffer solution (pH 6.8) was used as an anolyte. The CO_2-saturated phosphate buffer solution (pH 6.8) containing MV (100 mM) and CbFDH (7.5 μM) was used as a catholyte. The amount of formate production in this system was measured by ionic chromatography. Furthermore, for determination of the

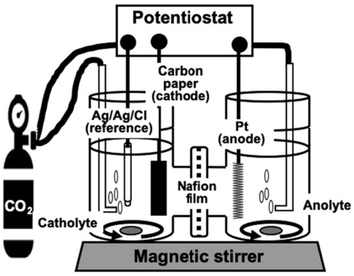

Fig. 11 Schematic representation for the electrochemical CO_2 reduction to formate using CbFDH and MV.

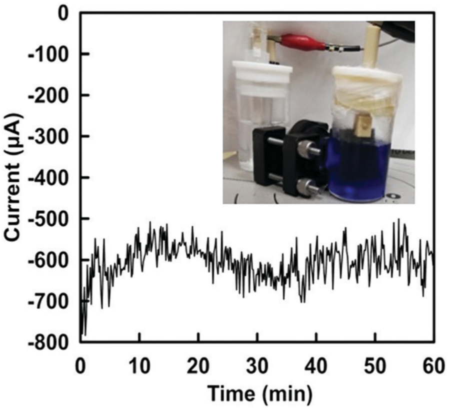

Fig. 12 Time-dependence of the current changes in the H-type electrochemical cell consisting of CO_2-saturated phosphate buffer as an anolyte and CO_2-saturated phosphate buffer containing MV and CbFDH as a catholyte under a continuously applied potential at −660 mV *vs.* Ag/AgCl. The inset shows the change of the catholyte under continuous potential application.

$MV^{+\bullet}$ concentration produced from the UV-visible absorption spectrum (SHIMADZU, MultiSpec-1500), an H-type cell with a 1 cm quartz cell on the cathodic side was used. $MV^{+\bullet}$ concentration was determined using the absorbance at 605 nm with a molar absorption coefficient $\varepsilon_{605} = 13\,500\ M^{-1}\ cm^{-1}$.[51]

Fig. 12 shows the time-dependence of current changes in the H-type electrochemical cell consisting of CO_2-saturated phosphate buffer as an anolyte and CO_2-saturated phosphate buffer containing MV and CbFDH as a catholyte under continuously applied potential at −660 mV *vs.* Ag/AgCl.

As shown in Fig. 12, an average current of −600 μA was constantly observed under a continuously applied potential at −660 mV *vs.* Ag/AgCl. The inset photograph in Fig. 12 also showed that the color of the solution changed from colorless to blue due to $MV^{+\bullet}$ production. After 1 h of continuously applied potential, 5.3 μM of formate production was observed. Considering that the $MV^{+\bullet}$ concentration by electrochemical reduction (*ca.* 1.0 mM) is higher than the apparent K_m value calculated from enzymatic kinetic analysis, the formate production rate (0.09 μM min^{-1}) was lower than that of the system of dithionite-reduced MV and CbFDH (*ca.* 15 μM min^{-1} at 1.0 mM of $MV^{+\bullet}$) shown in Fig. 4. The Faraday efficiency calculated from the amount of $MV^{+\bullet}$ produced and the current value was estimated to be *ca.* 85%.

Next, the CO_2 saturated phosphate buffer containing MV as a catholyte was electrochemically reduced in advance under a continuously applied potential at −660 mV *vs.* Ag/AgCl for 1 h, and then CbFDH was added to investigate the CO_2 to formate. However, no formate production is observed in this condition.

Finally, a constant potential at −660 mV *vs.* Ag/AgCl was applied to the CO_2-saturated phosphate buffer containing MV and CbFDH as a catholyte for 1 h, and then sodium dithionite was added in an attempt to reduce CO_2 to formate. After addition of sodium dithionite for 1 h, 189 μM of formate was produced.

When $MV^{+\bullet}$ is used as a co-enzyme for CbFDH, CO_2 reduction to formate with CbFDH requires two molecules of $MV^{+\bullet}$.

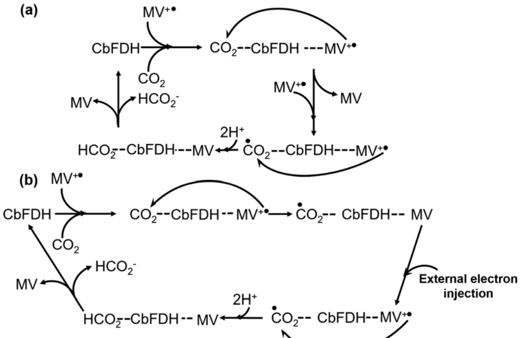

Fig. 13 Proposed mechanisms for the CO_2 reduction to formate with CbFDH and two molecules of $MV^{+\bullet}$.

From the results of electrochemical experiments, in addition to the mechanism in Fig. 5, two mechanisms were proposed for the CO_2 reduction to formate with CbFDH and $MV^{+\bullet}$ as shown in Fig. 13(a) and (b). The major difference among the three mechanisms is that, in the mechanism in Fig. 5, two molecules of $MV^{+\bullet}$ are bound to CbFDH simultaneously, in the mechanism in Fig. 13(a), $MV^{+\bullet}$ is sequentially bound to CbFDH, and in the mechanism in Fig. 13(b), MV bound to CbFDH is re-reduced by external electron injection. Each mechanism process according to the previous report based on the photoelectrochemical studies,[52] is as follows.

Mechanism in Fig. 5

(1) Tow molecules of $MV^{+\bullet}$ simultaneously bind to the catalytic active site of CbFDH to form the CbFDH–$2MV^{+\bullet}$ complex.

(2) The two electrons transfer from two $MV^{+\bullet}$s to the CO_2 binding site of CbFDH in the complex.

(3) CO_2 reduces to formate with $CbFDH^-$–2MV.

(4) Tow MVs dissociate from the CbFDH–2MV complex.

Mechanism (a)

(1) $MV^{+\bullet}$ binds to the catalytic active site of CbFDH to form the CbFDH–$MV^{+\bullet}$ complex.

(2) The electron transfers from $MV^{+\bullet}$ to the CO_2 binding site of CbFDH in the complex.

(3) MV dissociates from the CbFDH–MV complex.

(4) Second $MV^{+\bullet}$ binds to the catalytic active site of CbFDH.

(5) The electron transfers from $MV^{+\bullet}$ to the CO_2 binding site of CbFDH in the complex.

(6) CO_2 reduces to formate with CbFDH–MV.

(7) MV dissociates from the CbFDH–MV complex.

Mechanism (b)

(1) $MV^{+\bullet}$ binds to the catalytic active site of CbFDH to form the CbFDH–$MV^{+\bullet}$ complex.

(2) The electron transfers from $MV^{+\bullet}$ to the CO_2 binding site of CbFDH in the complex.

(3) Accepting electrons from the electrode, the MV moiety of the CbFDH–MV complex is re-reduced to form CbFDH–$MV^{+\bullet}$.

(4) The electron transfers from $MV^{+\bullet}$ to the CO_2 binding site of CbFDH in the complex.

(5) CO_2 reduces to formate with CbFDH–MV.

(6) MV dissociates from the CbFDH–MV complex.

The CO_2 reduction to formate did not proceed even when MV was electrochemically reduced to produce a large excess of $MV^{+\bullet}$ with respect to CbFDH. That is, it is shown that two molecules of $MV^{+\bullet}$ simultaneously bind to CbFDH and then the CO_2 reduction to formate (mechanism shown in Fig. 5) does not proceed. External electron injection is required for the CO_2 reduction to formate, based on the results of catalytic current observation in CV measurement shown in Fig. 10 and formate production under constant potential application (−660 mV *vs.* Ag/AgCl) in the CO_2-saturated buffer solution containing MV and CbFDH. From the experimental result of adding CbFDH after electrochemically producing excess $MV^{+\bullet}$, the mechanism of sequentially binding $MV^{+\bullet}$ to CbFDH as shown in Fig. 13(a) was also rejected. When the solution containing MV and CbFDH was electrochemically treated and then sodium dithionite was added, formate production after 1 h incubation (189 μM) was increased compared with that under constant potential application (−660 mV *vs.* Ag/AgCl) (5.3 μM). These results suggest that the CO_2 reduction to formate by $MV^{+\bullet}$ and CbFDH depends on the external electron injection source. In other words, it is presumed that the process for the external electron injection to MV bound to CbFDH contributes to the reduction rate of CO_2 to formate. Thus, it is suggested that the CO_2 reduction to formate with CbFDH and $MV^{+\bullet}$ proceeds with mechanism (b), as shown in Fig. 13.

To qualitatively prove this process, the CbFDH-catalyzed CO_2 reduction to formate in the presence of sodium dithionite below MV concentration was investigated. Fig. 14 shows the Lineweaver–Burk plot for CbFDH-catalyzed CO_2 reduction to formate in the system containing MV, CbFDH (7.5 μM) under various concentrations of sodium dithionite (100, 500 μM and 160 mM).

No change in the apparent K_m value of $MV^{+\bullet}$ for CbFDH in the CO_2 reduction to formate was observed at any sodium dithionite concentration. However, the gradient of the Lineweaver–Burk plot tended to increase as the concentration of added sodium dithionite decreased. This trend in the gradient change indicates a typical sequential process for binding of $MV^{+\bullet}$ to CbFDH and subsequent electron transfer from sodium dithionite.

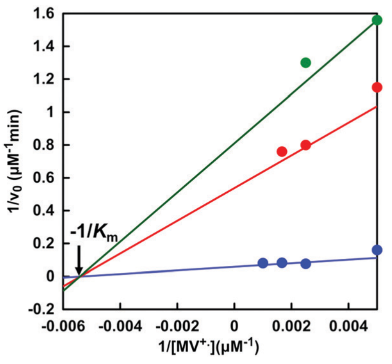

Fig. 14 Lineweaver–Burk plot for CbFDH-catalyzed CO_2 reduction to formate in the system containing MV, CbFDH (7.5 μM) and sodium dithionite. The concentrations of sodium dithionite: 100 μM: green, 500 μM: red, and 160 mM: blue.

In addition, the possibility that double electron-reduced MV (MV^0) functions as a co-enzyme for CbFDH in the CO_2 reduction to formate was investigated using an electrochemical method. The second reduction potential for MV was estimated to be −1.05 V *vs.* Ag/AgCl. The phosphate buffer containing MV as a catholyte was electrochemically reduced in advance under continuously applied potential at −1.05 V *vs.* Ag/AgCl for 1 h, and then CO_2 gas was introduced into a catholyte. Finally, CbFDH was added to investigate the CO_2 reduction to formate. However, no formate production is observed under this condition. Thus, it shows that the CO_2 reduction to formate does not proceed by donating two electrons from MV^0 directly to CbFDH.

Finally, the effect of CO_2 concentration on the formate production catalyzed by CbFDH with MV is mentioned. In many previous studies, bicarbonate has been considered as a CO_2 equivalent substrate for CbFDH-catalyzed formate production. We reported that formate production with CbFDH in the presence of NADH was investigated in solutions with different ratios of CO_2, bicarbonate and carbonate.[53] The reaction rate of formate production with CbFDH increased in proportion to the concentration of CO_2 in the reaction solution. On the other hand, the formate production with CbFDH was suppressed in proportion to the concentration of bicarbonate or carbonate in the reaction solution. Thus, CbFDH was found to catalytically reduce only CO_2 to formate among the three types of carbonate species. On the other hand, unfortunately, it is technically difficult to control the CO_2 concentration in the buffer solution containing sodium dithionite, and the concentration-dependence of CO_2 on CbFDH-catalyzed CO_2 reduction to formate with $MV^{+\bullet}$ the could not be mentioned. Since the focus of this study is on the interaction between $MV^{+\bullet}$ and sodium dithionite with CbFDH, the CO_2 concentration is in a condition of large excess (*ca.* 75 mM) with respect to CbFDH. Moreover, no formate production was observed under the condition of MV, sodium dithionite and CbFDH without CO_2.

Docking simulation for $MV^{+\bullet}$ binding to CbFDH

The binding mode of $MV^{+\bullet}$ to CbFDH was estimated by using the Autodock simulation. The $MV^{+\bullet}$, whose structure was optimized by DFT calculations, was docked into the substrate binding pocket of CbFDH (PDB ID: 5DN9), in which an azide ion was replaced with a CO_2 molecule. From the simulation, 47 clusters (total of 200 conformations) ranked by the lowest binding energy were obtained. The binding energy distribution in each cluster is shown in Fig. 15. Among these binding modes, $MV^{+\bullet}$s in 5 clusters (total of 68 conformations) were bound within 10 Å from CO_2 in CbFDH, while the others were around the entrance of the substrate binding pocket.

The structures of $MV^{+\bullet}$ in the 5 clusters are shown in Fig. 16. The lowest binding energy (LBE) of $MV^{+\bullet}$ and its distance between the methyl-group of $MV^{+\bullet}$ and CO_2 ($D(CH_3–CO_2)$) in each cluster are listed in Table 1. In the simulation results, 7 structures similar to the binding state of Run 167, in which $MV^{+\bullet}$ binds to the inner part of the substrate binding pocket of

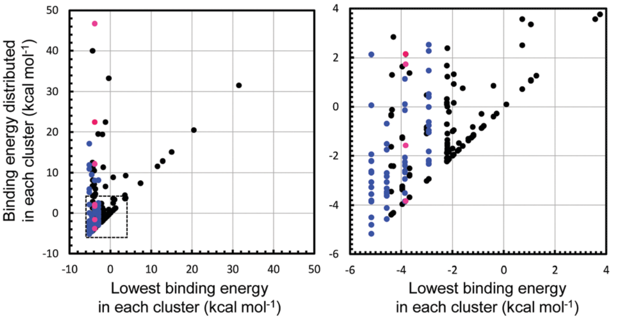

Fig. 15 The binding energy distribution of $MV^{+\bullet}$ with CbFDH simulated by Autodock. The right-side of the graph is an enlargement of the part surrounded by the dotted line in the left one. Pink circles are the cluster including Run 167, and blue circles are the clusters including Runs 29, 129, 1 and 139.

Table 1 $MV^{+\bullet}$ bound within 10 Å from CO_2 in CbFDH simulated by Autodock

Rank^a	Run^b	Num^c	LBE^d (kcal mol^{-1})	$D(CH_3–CO_2)^e$ (Å)
1	29	18	−5.17	7.01
2	129	13	−4.57	6.25
7	1	13	−3.86	6.19
8	167	7	−3.83	3.80
11	139	17	−2.93	9.10

^{a} Ranked by the lowest binding energy of clusters. ^{b} Run number that shows the lowest binding energy within each cluster. ^{c} Number of structures within each cluster. ^{d} The lowest binding energy within each cluster. ^{e} Distance between methyl-groups of $MV^{+\bullet}$ and CO_2.

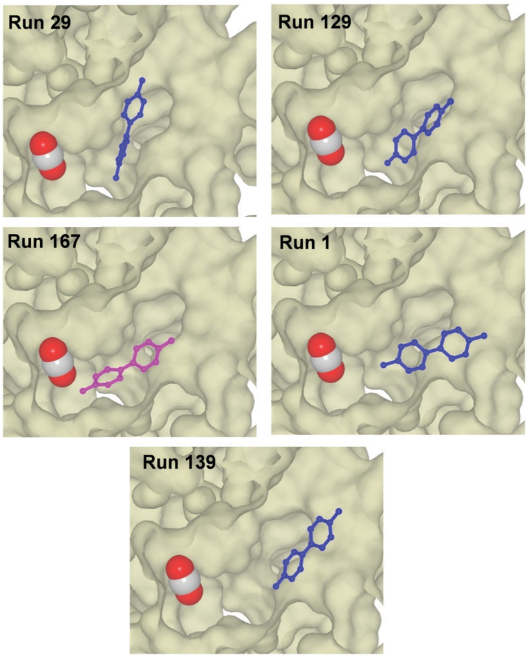

Fig. 16 Simulated $MV^{+\bullet}$ orientation at the substrate binding site of CbFDH by Autodock. CO_2 is shown as a ball model, $MV^{+\bullet}$ is shown as a ball and stick model, and the substrate binding site of CbFDH is shown as the contact surfaces.

CbFDH, were obtained. In these binding states, $MV^{\bullet}$ was close to CO_2 (∼4 Å). Besides, 61 structures similar to the binding state shown as Run 29, Run 129, Run 1, and Run 139 in Fig. 16 were obtained in the state for $MV^{+\bullet}$ binding from the middle of the substrate binding pocket of CbFDH to the vicinity of the entrance. In these binding states, $MV^{+\bullet}$ was 6–10 Å away from CO_2. These results suggest that $MV^{+\bullet}$ binds more easily to the middle of the substrate binding pocket of CbFDH than to the inner part when $MV^{+\bullet}$ is inserted within the substrate binding pocket.

Electron transfer ability of $MV^{\bullet}$ binding to CbFDH estimated by density functional theory (DFT)

Based on the conformation in five clusters, the total energy calculations of $MV^{+\bullet}$ and MV were performed using density functional theory (DFT). From the calculations, the energy level of the singly occupied molecular orbital (E_{SOMO}) and the electron transfer enthalpy (ETE) of $MV^{+\bullet}$ were estimated. These are used as the indexes of electron donation and acceptor abilities. The higher the E_{SOMO}, the higher the reactivity of the radical species. Also, the smaller the ETE value, the easier the electron donation to the acceptor is. E_{SOMO} and ETE obtained from DFT calculations are summarized in Table 2.

In the bound state of $MV^{+\bullet}$ to CbFDH, the structure of Run 167 showed the highest E_{SOMO} and the smallest ETE among the 5 structures, which were calculated to be −5.68 EV and 418 kJ mol^{-1}, respectively. The $MV^{+\bullet}$ of Run 167 is bound at a short distance (∼3.8 Å) to CO_2 in the inner part of the substrate binding pocket of CbFDH (Fig. 16). On the other hand, E_{SOMO} (−6.69 to −6.86 eV) and ETE values (503–532 kJ mol^{-1}) of the other structures, which bind around the middle of the substrate binding pocket of CbFDH (Fig. 16), were lower and higher, respectively, than those of the Run 167 structure. Furthermore, E_{SOMO} of $MV^{+\bullet}$ in an aqueous medium was −6.19 eV calculated using CPCM, when water was used as the solvent. The potential level was also lower than that of the Run 167 structure. These results indicate that the $MV^{+\bullet}$ bound to the inner part of the substrate binding pocket of CbFDH shows a high electron-donating ability compared to the $MV^{+\bullet}$ in aqueous medium and bound to the entrance or the middle of the substrate binding pocket of CbFDH.

The high E_{SOMO} of Run 167 is due to the structural distortion of $MV^{+\bullet}$. Among the five structures of $MV^{+\bullet}$ investigated in this study, the correlations between the dihedral angles of two aromatic rings of $MV^{+\bullet}$ and the E_{SOMO} values or the ETE values were observed (Table 2). The highly distorted structure of Run 167 is caused by the interaction with the surface of the substrate binding pocket of CbFDH (Fig. 16). The space of the substrate binding pocket around the CO_2 molecule is narrower than in the middle and around the entrance of the pocket. Therefore, when the $MV^{+\bullet}$ molecule binds closely to the CO_2 molecule, the $MV^{+\bullet}$ is structurally distorted due to its interaction with the protein surface. These results suggest that the substrate binding site of CbFDH controls the binding structure and electron donation ability of the $MV^{+\bullet}$.

The ETE of dithionite in the hydrophobic environment similar to the substrate binding pocket was calculated to be 439 kJ mol^{-1}. Compared to this value, $MV^{+\bullet}$ bound to the

Table 2 ETE and the HOMO level of the MV$^{+\bullet}$ in CbFDH

Rank	Run	ETE[a] (kJ mol^{-1})	E_{SOMO}[b] (eV)	DA[c] (°)
1	29	503	−6.69	30.8
2	129	516	−6.73	26.9
7	1	532	−6.86	2.5
8	167	418	−5.68	88.7
11	139	528	−6.81	15.3

[a] ETE = $H(\mathrm{MV}) + H(\mathrm{e}^-) - H(\mathrm{MV}^{+\bullet})$, where H(MV), and $H(\mathrm{MV}^{+\bullet})$ are the total enthalpy values of MV and MV$^{\bullet}$, which were estimated from the calculation using ωB97XD/6-311++g(d,p) with CPCM(diethyl ether), and $H(\mathrm{e}^-)$ is the enthalpy of electrons, which was taken from ref. 57. [b] Energy level of the SOMO of MV$^{+\bullet}$. [c] Dihedral angle between two aromatic rings.

entrance or the middle of the substrate binding pocket of CbFDH (Run 29, 129, 1, and 139) had high ETE as shown in Table 2, suggesting that these MVs play a role as the electron acceptor from dithionite rather than donating electrons to CO_2.

According to the difference in E_{SOMO} and ETE, together with the distribution of the docking orientation simulated by Autodock, CbFDH is assumed to form a complex with a MV$^{+\bullet}$ moiety, which dominantly binds around the entrance of the substrate binding pocket, and some of the MV$^{+\bullet}$ moieties can bind near CO_2 in the inner part of the substrate binding pocket, where MV$^{+\bullet}$ donates an electron to CbFDH. In this case, the CO_2 reduction is strongly influenced by the binding affinity of MV$^{+\bullet}$ to the inner part of substrate binding pocket of CbFDH rather than the electron-donating property of the MV$^{+\bullet}$.

Conclusion

In order to elucidate the two-electron supply process using MV$^{+\bullet}$ as a co-enzyme in the reduction process of CO_2 to formate catalyzed by CbFDH, we attempted to clarify the mechanism by experimental (enzyme reaction kinetics, and electrochemical methods) and quantum chemical analyses (docking simulation and DFT calculation). Kinetic parameters obtained from the enzymatic kinetic analysis metric revealed an index of affinity of MV$^{+\bullet}$ for CbFDH in the CO_2 reduction to formate. However, in this reaction system, sodium dithionite is excessive as a reducing agent. Therefore, the analysis of the reaction using dithionite-reduced MV does not lead to the clarification of the two-electron supply mechanism from MV$^{+\bullet}$ to CbFDH. From the results of the electrochemical analysis, it was predicted that only one molecule of MV$^{+\bullet}$ was bound to CbFDH, and the MV bound to CbFDH needs to be re-reduced by the electron source outside of CbFDH to supply the second electron in the CO_2 reduction to formate. From the results of docking simulation and DFT calculations, it was shown that one molecule of MV$^{+\bullet}$ bound to the position close to CO_2 in the inner side of substrate binding pocket of CbFDH, contributing to the two-electron CO_2 reduction to formate. We propose that clarification of the mechanism of two-electron CO_2 reduction to formate with CbFDH and MV$^{+\bullet}$ gives guidelines to develop new CO_2 reduction systems using biocatalyst and effective co-enzymes.

Experimental

Materials

FDH from *Candida boidinii* (CbFDH) was purchased from Roche Diagnostics K.K. The molecular weight of CbFDH was estimated to be 74 kDa.[54] MV dichloride, 4,4′-bipyridine, 1,5-dibromopentane and methyl iodide were purchased from Tokyo Kasei Co. Ltd. The proton permeable film, Nafion® 115 film, was obtained from Sigma-Aldrich Co. Ltd. Carbon fabric paper (CFP) (TGP-H-030) was obtained from TORAY INDUSTRIES, INC. The other chemical regents were of analytical grade or the highest grade available.

Preparation of MVC$_5$VM

1,5-Bis(4′-methyl-4,4-bipyridin-4-yl)pentane (MVC$_5$VM) was synthesized from 1-methyl-4,4′-bipyridinium iodide and 1,5-dibromopentane as shown in Fig. 17.

1-Methyl-4,4′-bipyridinium iodide was prepared from 4,4′-bipyridine and methyl iodide. 4,4′-Bipyridine (0.16 mol) and methyl iodide (0.18 mol) were dissolved in 400 mL of acetone and stirred at room temperature for 24 h. A yellow precipitate was collected by suction filtration and washed with acetone. The desired product was recrystallized from ethanol/water and then dried under vacuum overnight. MVC$_5$VM was prepared from 1-methyl-4,4′-bipyridinium iodide and 1,5-dibromopentane. 1-Methyl-4,4′-bipyridinium iodide (0.34 mmol) was dissolved in 200 mL of acetonitrile, then 1,5-dibromopentane (0.13 mol) was added to this solution. The reaction mixture was heated to reflux for 24 h. A yellow precipitate was collected by suction filtration, washed with acetonitrile and dried under vacuum overnight. The desired product was recrystallized from ethanol.

The purity of MVC$_5$VM prepared was checked by proton nuclear magnetic resonance spectroscopy using a ^{1}H-NMR Varian GEMINI-200 system. ^{1}H-NMR in D_2O: δ (ppm) 1.40 (2H, quint, J = 5.5 Hz), 1.95 (4H, tt, J = 7.6, 5.5 Hz), 4.30 (6H, s), 4.52 (4H, t, J = 7.6 Hz), 8.30–8.35 (8H, 8.32 (ddd, J = 5.7, 1.5, 0.5 Hz), 8.32 (ddd, J = 5.7, 1.4, 0.5 Hz)), 9.00–9.05 (8H, 9.02 (ddd, J = 5.7, 2.0, 0.5 Hz), 9.02 (ddd, J = 5.7, 2.0, 0.6 Hz)).

CO_2 reduction to formate with dithionite-reduced viologen and CbFDH

The CO_2 reduction to formate with dithionite MV or MVC$_5$VM and CbFDH was carried out as follows. MV$^{+\bullet}$ or MV$^{\bullet}$C$_5$$^{\bullet}$VM was prepared with sodium dithionite using the following method.

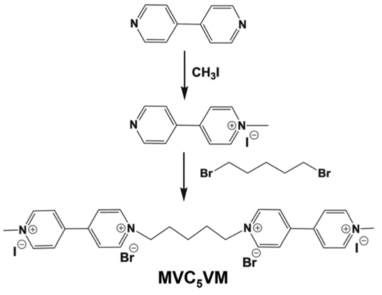

Fig. 17 Synthesis scheme for 1,5-bis(4′-methyl-4,4-bipyridin-4-yl)pentane (MVC$_5$VM).

First, sodium dithionite powder was added into a quartz cell and then deaerated using a vacuum pump and then flushed with CO_2 gas. A solution containing MV or MVC_5VM in 5.0 mL of 50 mM sodium pyrophosphate buffer (pH 7.4) was deaerated by freeze–pump–thaw cycles repeated 6 times and then flushed with CO_2 gas for 5 min. To prepare $MV^{+\bullet}$ or $MV^{+\bullet}C_5{}^{+\bullet}VM$ solution, 3.0 mL of MV or MVC_5VM solution was added into a quartz cell and reacted with sodium dithionite (160 mM) under continuously flowing CO_2 gas. The reaction was started by injection of CbFDH solution (7.5 μM) to $MV^{+\bullet}$ or $MV^{+\bullet}C_5{}^{+\bullet}VM$ in 3.0 mL of 50 mM CO_2-saturated sodium pyrophosphate buffer (pH = 7.4). The amount of formate was determined using ion chromatography (Dionex ICS-1100; electrical conductivity detector) with an ion exclusion column (Thermo ICE AS1; column length: 9 × 150 mm; composed of a 7.5 μm cross-linked styrene/divinylbenzene resin with functionalized sulfonate groups). 1.0 mM of octane sulfonic acid and 5.0 mM of tetrabutylammonium hydroxide were used as an eluent and a regenerant, respectively. Lowering of pH by addition of sodium dithionite was suppressed by using sodium pyrophosphate buffer solution (pH 7.4), indicating that the stability of FDH was retained in the sodium dithionite-saturated solution. The concentration of formate was measured for 1 min to estimate the initial rate of the CO_2 reduction to formate.

Cyclic voltammogram measurements

The CV curves of MV and MV + CbFDH in CO_2-saturated 0.1 M phosphate buffer (pH 6.8) at a scan rate of 10 mV s^{-1} (*vs.* Ag/AgCl (1 M KCl)) were measured using a potentiostat (Hokuto Denko HZ-3000). Grassy carbon and platinum wire electrodes were used as the working and counter electrodes, respectively. Ag/AgCl electrode was used as the reference electrode.

CO_2 reduction to formate with electrochemically reduced MV and CbFDH

The CO_2 reduction to formate with electrochemically reduced MV and CbFDH was carried out as follows. In constant potential CO_2 reduction to formate using CbFDH and MV, an H-type electrochemical cell was used. The cell volume is 18 mL. Platinum wire, carbon fabric paper (CFP) (electrode area: 3.75 cm^2) and Ag/AgCl electrodes were used as the anode, cathode and reference electrodes, respectively. The CO_2-saturated phosphate buffer solution (pH 6.8) and the CO_2-saturated phosphate buffer solution (pH 6.8) containing MV (100 mM) and CbFDH (7.5 μM) were used as the anolyte and catholyte, respectively. The volumes of the anolyte and catholyte were 10 mL, respectively. The chambers of the anode and cathode sides were connected *via* Nafion® 115. Photocurrent was measured with an electrochemical analyzer (ALS1200C BAS Inc.). The amount of formate was detected using ion chromatography (Dionex ICS-1100; electrical conductivity detector) with an ion exclusion column (Thermo ICE AS1; column length: 9 × 150 mm; composed of a 7.5 μm cross-linked styrene/divinylbenzene resin with functionalized sulfonate groups). 1.0 mM octane sulfonic acid and 5.0 mM tetrabutylammonium hydroxide were used as an eluent and a regenerant, respectively.

For determination of the concentration of $MV^{+\bullet}$ produced in the cathode side, a UV-vis spectrum was obtained with the molar extinction coefficient at 605 nm ($\varepsilon = 1.3 \times 10^4\ M^{-1}\ cm^{-1}$) using a spectrophotometer (SEC200 BAS Inc.). The cell volumes of the chambers of anode and cathode sides were 18 and 5.0 mL, respectively.

Docking simulation and DFT calculations

For preparing the molecular model of CbFDH for docking simulations, the crystal structure of CbFDH was obtained from the Protein Data Bank (PDB) database (PDB ID: 5DN9).[55] The protein structure of 5DN9 contains NAD^+ and N_3 as substrates. For constructing a CbFDH model used for docking simulation, NAD^+ and water molecules were removed, and N_3 was replaced with CO_2 because the CbFDH–NAD^+–N_3 complex has been reported as the transition-state analogue of the formate dehydrogenation to CO_2 by CbFDH.[56] In the transition model, a reactant (formate anion) and a product (CO_2) are located at the same place with N_3. Besides, for preparing the molecular model of MV, the molecular structure of MV was drawn using GaussView 5.0. For the calculations, the amino and carboxyl groups were protonated and deprotonated, respectively. The MV model was optimized by DFT calculation using the ωB97XD functional and the 6-311++G(d,p) basis set in Gaussian 09.[57]

By using the molecular models, docking simulation was performed using Autodock 4.2.[58] As the docking site, the grid size was set to 40 × 40 × 40 points with a grid spacing of 0.608 Å centered on the original ligand in the crystal structure of CbFDH. The grid box included the entire substrate binding pocket of CbFDH and provided enough space for the ligand translational and rotational walk. To search molecular dockings, the Lamarckian genetic algorithm and the pseudo-Solis and Wets methods were applied for minimization using default parameters. The standard docking protocol for rigid and flexible ligand docking was performed. In the binding of MV to CbFDH, some amino acid residues composed of the substrate binding pocket of CbFDH possibly move and fit MV. Thus, V93, N119, V123, R174, I175, T256, R258, H311, S313, and Y358 of CbFDH, which are oriented on the surface of the substrate binding pocket, were selected as the flexible amino acid residues. The molecular models were subjected to 200 independent runs per ligand, and other parameters were set to the default values.

The ETE of CbFDH-bound forms of $MV^\bullet$ simulated using Autodock was calculated using the following equation.

$$\mathrm{ETE} = H(\mathrm{MV}) + H(\mathrm{e}^-) - H(\mathrm{MV}^\bullet)$$

where $H(\mathrm{MV})$ and $H(\mathrm{MV}^\bullet)$ are the total enthalpies of MV and $MV^\bullet$ at 298 K, respectively. These enthalpies were estimated from the results of the single-point calculation using the DFT method described above. In the calculations, the solvation effects were taken into account using the conductor-like polarizable continuum model (CPCM). As solvents, diethyl ether and water (relative permittivity = 4.3 and 78.4, respectively) were chosen as the models of the hydrophobic substrate binding pocket and aqueous medium, respectively. The enthalpies were estimated by the approximation of the molecules in the gas phase, and contained three-dimensional translation energy, three directional rotation energy, and a PV term as the ideal gas. These values are not the same as those inside the protein, but would be exactly canceled out because $H(\mathrm{MV})$ and $H(\mathrm{MV}^*)$ contain the same values. $H(\mathrm{e}^-)$, the enthalpy of electrons, was taken from the literature.[59]

Conflicts of interest

There are no conflicts to declare.

Acknowledgements

This work was partially supported by a Grant-in-Aid for Scientific Research on Innovative Areas "Artificial Photosynthesis (2406)", "Innovations for Light-Energy Conversion (4906)", the Fund for the Promotion of Joint International Research (Fostering Joint International Research (B))(19KK0144), and the joint usage/research program of the Artificial Photosynthesis, Osaka City University.

Notes and references

1 V. I. Tishkov and V. O. Popov, *Biochemistry*, 2004, **69**, 1252.
2 R. Wichmann, C. Wandrey, A. F. Buckmann and M. R. Kula, *Biotechnol. Bioeng.*, 1981, **23**, 2789.
3 W. Hummel and M. R. Kula, *Eur. J. Biochem.*, 1989, **184**, 1.
4 H. Zhao and W. A. van der Donk, *Curr. Opin. Biotechnol*, 2003, **14**, 583.
5 J. G. Ferry, *FEMS Microbiol. Rev.*, 1990, **7**, 377.
6 Y. Amao, *J. CO2 Util.*, 2018, **26**, 623.
7 H. Choe, J. C. Joo, D. H. Cho, M. H. Kim, S. H. Lee, K. D. Jung and Y. H. Kim, *PLoS One*, 2014, **9**, e103111.
8 J. H. Kim, D. H. Nam and C. B. Park, *Curr. Opin. Biotechnol.*, 2014, **28**, 1.
9 S. K. Kuk, R. K. Singh, D. H. Nam, R. Singh, J. K. Lee and C. B. Park, *Angew. Chem., Int. Ed.*, 2017, **56**, 3827.
10 H. Wu, C. Tian, X. Song, C. Liu, D. Yang and Z. Jiang, *Green Chem.*, 2013, **15**, 1773.
11 R. K. Yadav, J.-O. Baeg, G. H. Oh, N.-J. Park, K.-J. Kong, J. Kim, D. W. Hwang and S. K. Biswas, *J. Am. Chem. Soc.*, 2012, **134**, 11455.
12 X. Ji, Z. Su, P. Wang, G. Ma and S. Zhang, *ACS Nano*, 2015, **9**, 4600.
13 R. K. Yadav, G. H. Oh, N.-J. Park, A. Kumar, K.-J. Kong and J.-O. Baeg, *J. Am. Chem. Soc.*, 2014, **136**, 16728.
14 K. J. Shah and T. Imae, *J. Mater. Chem. A*, 2017, **5**, 9691.
15 Y. Amao, *Chem. Lett.*, 2017, **46**, 780.
16 Y. Amao, *Sustainable Energy Fuels*, 2018, **2**, 1928.
17 D. Mandler and I. Willner, *J. Chem. Soc., Perkin Trans. 2*, 1988, 997.
18 I. Willner and D. Mandler, *J. Am. Chem. Soc.*, 1989, **111**, 1330.
19 I. Willner, N. Lapidot, A. Riklin, R. Kasher, E. Zahavy and E. Katz, *J. Am. Chem. Soc.*, 1994, **116**, 1428.
20 I. Willner, I. Willner and N. Lapidot, *J. Am. Chem. Soc.*, 1990, **112**, 6438.
21 R. Miyatani and Y. Amao, *Biotechnol. Lett.*, 2002, **24**, 1931.
22 R. Miyatani and Y. Amao, *J. Mol. Catal. B: Enzym.*, 2004, **27**, 121.
23 R. Miyatani and Y. Amao, *J. Jpn. Pet. Inst.*, 2004, **47**, 27.
24 Y. Amao, R. Abe and S. Shiotani, *J. Photochem. Photobiol., A*, 2015, **313**, 149.
25 I. Tsujisho, M. Toyoda and Y. Amao, *Catal. Commun.*, 2006, **7**, 173.
26 M. Kodaka and Y. Kubota, *J. Chem. Soc., Perkin Trans. 2*, 1999, 891.
27 S. Ikeyama and Y. Amao, *Sustainable Energy Fuels*, 2017, **1**, 1730.
28 S. Ikeyama and Y. Amao, *Photochem. Photobiol. Sci.*, 2018, **17**, 60.
29 R. Miyatani and Y. Amao, *Photochem. Photobiol. Sci.*, 2014, **3**, 681.
30 Y. Amao and T. Watanabe, *Chem. Lett.*, 2004, **33**, 1544.
31 Y. Amao and T. Watanabe, *Appl. Catal., B*, 2009, **86**, 109.
32 Y. Amao and R. Kataoka, *Catal. Today*, 2018, **307**, 243.
33 Y. Amao and S. Ikeyama, *Chem. Lett.*, 2015, **44**, 1182.
34 S. Ikeyama and Y. Amao, *Chem. Lett.*, 2016, **45**, 1259.
35 S. Ikeyama and Y. Amao, *ChemCatChem*, 2017, **9**, 833.
36 S. Ikeyama and Y. Amao, *New J. Chem.*, 2018, **42**, 15556.
37 S. Ikeyama, R. Abe, S. Shiotani and Y. Amao, *Chem. Lett.*, 2016, **45**, 907.
38 S. Ikeyama, R. Abe, S. Shiotani and Y. Amao, *Bull. Chem. Soc. Jpn.*, 2018, **91**, 1369.
39 P. M. S. Monk, *The viologens: physicochemical properties, synthesis, and applications of the salts of 4,4′-bipyridine*, Wiley, Hoboken, 1998.
40 D. Small, V. Zaitsev, Y. Jung, S. V. Rosokha, M. Head-Gordon and J. K. Kochi, *J. Am. Chem. Soc.*, 2004, **126**, 13850.
41 S. Suzuki, Y. Morita, K. Fukui, K. Sato, D. Shiomi, T. Takui and K. Nakasuji, *J. Am. Chem. Soc.*, 2006, **128**, 2530.
42 J. L. Zafra, L. Qiu, N. Yanai, T. Mori, M. Nakano, M. P. Alvarez, J. T. L. Navarrete, C. J. Glmez-Garcia, M. Kertesz, K. Takimiya and J. Casado, *Angew. Chem., Int. Ed.*, 2016, **55**, 14563.
43 Z. Mou, K. Uchida, T. Kubo and M. Kertesz, *J. Am. Chem. Soc.*, 2014, **136**, 18009.
44 J. J. Novoa, P. Lafuente, R. E. Del Sesto and J. S. Miller, *Angew. Chem., Int. Ed.*, 2001, **40**, 2540.
45 J. Jakowski and J. Simons, *J. Am. Chem. Soc.*, 2003, **125**, 16089.
46 J.-F. Penneau and L. L. Miller, *Angew. Chem., Int. Ed. Engl.*, 1991, **30**, 986.
47 J.-M. Lg, S. V. Rosokha and J. K. Kochi, *J. Am. Chem. Soc.*, 2003, **125**, 12161.
48 M. R. Geraskina, A. S. Dutton, M. J. Juetten, S. A. Wood and A. H. Winter, *Angew. Chem., Int. Ed.*, 2017, **56**, 9435.
49 T. Sagara and H. Eguchi, *Electrochim. Acta*, 2019, **295**, 215.
50 K. Sakai, B.-C. Hsieh, A. Maruyama, Y. Kitazumi, O. Shirai and K. Kano, *Sens. Biosens. Res.*, 2015, **5**, 90.
51 T. Watanabe and K. Honda, *J. Phys. Chem.*, 1982, **86**, 2617.

52 T. Ishibashi, M. Higashi, S. Ikeda and Y. Amao, *ChemCatChem*, 2019, **11**, 6227.

53 R. Sato and Y. Amao, *New J. Chem.*, 2020, **44**, 11922.

54 N. L. Allinger, *J. Am. Chem. Soc.*, 1977, **99**, 8127.

55 Q. Guo, L. Gakhar, K. Wickersham, K. Francis, A. Vardi-Kilshtain, D. T. Major, C. M. Cheatum and A. Kohen, *Biochemistry*, 2016, **55**, 2760.

56 J. N. Bandaria, C. M. Cheatum and A. Kohen, *J. Am. Chem. Soc.*, 2009, **131**, 10151.

57 M. J. Frisch, G. W. Trucks, H. B. Schlegel, G. E. Scuseria, M. A. Robb, J. R. Cheeseman, G. Scalmani, V. Barone, B. Mennucci, G. A. Petersson, H. Nakatsuji, M. Caricato, X. Li, H. P. Hratchian, A. F. Izmaylov, J. Bloino, G. Zheng, J. L. Sonnenberg, M. Hada, M. Ehara, K. Toyota, R. Fukuda, J. Hasegawa, M. Ishida, T. Nakajima, Y. Honda, O. Kitao, H. Nakai, T. Vreven, J. A. Montgomery Jr, J. E. Peralta, F. Ogliaro, M. Bearpark, J. J. Heyd, E. Brothers, K. N. Kudin, V. N. Staroverov, R. Kobayashi, J. Normand, K. Raghavachari, A. Rendell, J. C. Burant, S. S. Iyengar, J. Tomasi, M. Cossi, N. Rega, J. M. Millam, M. Klene, J. E. Knox, J. B. Cross, V. Bakken, C. Adamo, J. Jaramillo, R. Gomperts, R. E. Stratmann, O. Yazyev, A. J. Austin, R. Cammi, C. Pomelli, J. W. Ochterski, R. L. Martin, K. Morokuma, V. G. Zakrzewski, G. A. Voth, P. Salvador, J. J. Dannenberg, S. Dapprich, A. D. Daniels, O. Farkas, J. B. Foresman, J. V. Ortiz, J. Cioslowski and D. J. Fox, *Gaussian 09, Revision A.1*, Gaussian, Inc., Wallingford CT, 2009.

58 G. M. Morris, R. Huey, W. Lindstrom, M. F. Sanner, R. K. Belew, D. S. Goodsell and A. J. Olson, *J. Comput. Chem.*, 2009, **16**, 2785.

59 J. E. Bartmess, *J. Phys. Chem.*, 1993, **98**, 5648.